Hydrodynamic instability of elastic-plastic solid plates at the early stage of acceleration

A. R. Piriz*
E.T.S.I. Industriales, Instituto de Investigaciones Energéticas and CYTEMA, Universidad de Castilla-La Mancha, 13071 Ciudad Real, Spain

Y. B. Sun†
Institute of Modern Physics, Chinese Academy of Science, 730000 Lanzhou, People's Republic of China

N. A. Tahir
GSI Helmholtzzentrum für Schwerionenforschung Darmstadt, Planckstrasse 1, 64291 Darmstadt, Germany
(Received 17 December 2014; revised manuscript received 15 February 2015; published 9 March 2015)

A model is presented for the linear Rayleigh-Taylor instability taking place at the early stage of acceleration of an elastic-plastic solid, when the shock wave is still running into the solid and is driven by a time varying pressure on the interface. When the the shock is formed sufficiently close to the interface, this stage is considered to follow a previous initial phase controlled by the Ritchmyer-Meshkov instability that settles new initial conditions. The model reproduces the behavior of the instability observed in former numerical simulation results and provides a relatively simpler physical picture than the currently existing one for this stage of the instability evolution.

DOI: 10.1103/PhysRevE.91.033007 PACS number(s): 47.20.−k, 52.58.Hm, 52.50.Lp

I. INTRODUCTION

There is a growing interest in the hydrodynamic instabilities taking place in accelerated solids, namely Rayleigh-Taylor instability (RTI) and Ritchmyer-Meshkov instability (RMI), mainly because of the central role played by these instabilities in many experiments in high-energy-density physics (HEDP) [1–38]. In fact, hydrodynamic instabilities are of importance for determining the performance of many current and planned experiments directed to the study of equation of state and mechanical and thermophysical properties of matter [1–18], as well as experiments related to the examination of new approaches to inertial confinement fusion [19–23]. In particular, on the basis of the pioneering work by Barnes *et al.* [14,15] with solid plates accelerated by means of high explosives, intense research has been recently undertaken centered in the use of RTI for the evaluation of the yield strength of solids at high strain and high-strain-rate conditions [2–7]. More recently, also RMI has been considered for similar purposes [29,30,39–42].

Most of the theoretical work on hydrodynamic instabilities in accelerated media consider that the acceleration is driven by a constant pressure so that the early acceleration phase, taking place during the time when the shock wave is running into the plate, is dominated by the evolution of RMI. In such a case, RTI does not start until the rarefaction wave reflected at the rear face of the plate arrives back to the front face. In that moment the plate is accelerated as a whole and the instability becomes dominated by the RTI seeded by the perturbations left by the RMI evolving during the shock transit time in the previous early stage of the plate acceleration.

However, in most of the situations of interest in HEDP experiments the solid plate is driven by a highly transient pressure pulse that varies considerably during the shock transit time and causes the acceleration of the shocked material. Therefore, during this early stage the plate is also susceptible to being affected by RTI in addition to RMI. Such a situation has not been frequently considered in the literature. In fact, it has been investigated by Clarisse *et al.* [43] for the case of an ablation front by using a self-similar solution for describing the ideal gas mean flow profiles in order to take into account the unsteadiness and compressibility effects on the instability evolution.

For the case of accelerated solids, Swegle and Robinson [44] have performed two-dimensional numerical simulations for the case of a solid occupying a half-space, and with a sinusoidal perturbation imposed on the interface. In this work a shock wave is driven by a time-dependent pressure consisting of a linear ramp to the maximum pressure over the rise time of the pressure pulse, after which the pressure remains constant or decreases linearly to zero. In these simulations the effect of the pressure time dependence is studied by varying the time duration and the slope of the pressure ramp. The results were interpreted in terms of an acceleration instability, which was considered to produce phenomena that were without precedent in classical RTI. It was concluded that although the solid interface was accelerated "in a global sense," there was "no quantity which is strictly analogous to the acceleration of gravity g in RTI."

Part of the difficulty in assimilating the simulation results obtained in Ref. [44] to a known instability may have been due to the fact that at this early stage of the acceleration process both RMI and RTI are contributing to the interface instability. In fact, it should be expected that the interface instability will be controlled by RMI until the shock wave has separated from the interface a distance of the order of k^{-1} ($k = 2\pi/\lambda$, where λ is the perturbation wavelength) [45–50]. The latter is true even for the weakest shock waves, since RMI develops for any intensity of the shock including the case of an upstream Mach number equal to unity [45–47,50]. Therefore, even in the so-called shockless driven experiments in which the plate is quasi-isentropically accelerated by a tailored pressure

*roberto.piriz@uclm.es
†Present address: E.T.S.I. Industriales and Instituto de Investigaciones Energéticas, Universidad de Castilla-La Mancha, 13071 Ciudad Real, Spain.

pulse [3,4,7,14,15], a weak shock may be launched at the initial stage which would lead to the growth of interface perturbations as a consequence of the RMI. This would happen provided that the process of shock formation, as a consequence of the overlap of the weak compression waves launched from the interface, takes place within a distance shorter that k^{-1} [49].

After the shock wave has separated from the interface a distance of the order of k^{-1}, the RTI would dominate the perturbation growth caused by the interface acceleration produced by the time-varying pressure that drives the shock.

In this work we present an analytical model for the early stage of the RTI evolution occurring at the solid interface during the transit time of the shock wave inside the solid plate. This stage will be eventually preceded by a previous phase of RMI growth that would settle new initial conditions.

II. FORMULATION OF THE PROBLEM AND MODEL

A. Mean flow model

We consider an elastic-plastic (EP) solid of density ρ_0 occupying the half-space $y < 0$ as in Fig. 1 (actually a plate thick enough that, during the time span we are studying the problem, the shock wave has not yet achieved the rear face). On the free surface ($y = 0$), a time-dependent pressure $p_p(t)$ is applied for times $t \geqslant 0$. As a consequence, a shock wave is launched into the solid and it moves away from the interface with a velocity $U_s - u$ (where U_s and u are, respectively, the velocities of the shock and of the particles behind it in the laboratory reference frame). From the conservation laws, we have

$$\frac{\rho_s}{\rho_0} = \frac{U_s}{U_s - u}, \tag{1}$$

$$p_s = \rho_0 U_s u, \tag{2}$$

where ρ_s and p_s are, respectively, the density and the pressure immediately behind the shock, and we have neglected the pressure ahead of it. In addition, we assume that the wave velocity U_s and the particle velocity u are related by a linear relationship [51],

$$U_s = c_0 + su, \tag{3}$$

where c_0 and s are known material constants. Since in the present situation we are considering a shock propagating in a solid media, it must be relatively weak in order to avoid melting, so that we typically have $\sigma = 1 - \rho/\rho_0 \ll 1$. Furthermore, we assume isentropic flow behind the shock and a low enough compressibility in order to consider that in the momentum conservation equation the particle velocity u can be taken to be practically uniform. Actually, u will be rather uniform except for a highly compressible medium behind the shock, as can be noticed from the mass conservation equation:

$$\frac{d}{dt}(\ln \rho) = -\frac{\partial u}{\partial y} \approx 0. \tag{4}$$

Thus from Eqs. (2) and (3) we get the following relationship between the particle velocity u and the pressure $p_s(t)$ just behind the shock:

$$\frac{u(t)}{c_0} = \frac{1}{2s}\left(\sqrt{1 + \frac{4sp_s(t)}{\rho_0 c_0^2}} - 1\right). \tag{5}$$

We can relate the pressure $p_s(t)$ with the driving pressure $p_p(t)$ applied on the interface by using the momentum conservation equation:

$$\rho\frac{du}{dt} = \rho\left(\frac{\partial u}{\partial t} + u\frac{\partial u}{\partial y}\right) = -\frac{\partial p}{\partial y}, \tag{6}$$

where the convective derivative as well as the mechanical forces (described by the stress tensor) are negligible for the one-dimensional flow with $\partial u/\partial y \approx 0$ behind the shock. Therefore, in the interface reference frame, Eq. (6) becomes the hydrostatic equation and upon integration it yields

$$p_p = p_s + \rho g y_s, \quad g = \frac{du}{dt}, \tag{7}$$

where $p_s(t) = \rho_0 u(c_0 + su)$, and $y = y_s(t)$ is the instantaneous position of the wave in the interface reference frame:

$$-y_s = \int_0^t (U_s - u)dt = \int_0^t [c_0 + (s-1)u]dt. \tag{8}$$

For a given driving pressure $p_p(t)$, Eqs. (3), (7), and (8) lead to a nonlinear second-order differential equation for $y_s(t)$ which, together with Eqs. (1) to (3) yields $u(t)$, $U_s(t)$, and $p_s(t)$. However, without losing generality in our conclusions and in order to achieve considerable simplicity, we can impose a pressure time dependence $p_s(t)$ behind the shock and calculate the pressure $p_p(t)$ on the interface necessary to produce it from Eq. (7). Thus, from Eq. (5) we can get the acceleration of the medium behind the shock:

$$g(t) = \frac{du}{dt} = \frac{1}{\rho_0 c_0}\frac{1}{\sqrt{1 + \frac{4sp_s}{\rho_0 c_0^2}}}\frac{dp_s}{dt} = \text{const.} \tag{9}$$

A particularly simple case corresponds to the one with a constant acceleration $g = g_0$, and we will consider it in the following analysis of the plate instability. Therefore, from Eq. (2) we easily obtain the time dependence of the pressure just behind the shock wave:

$$p_s(t) = \rho_0 g_0 t(c_0 + sg_0 t). \tag{10}$$

Actually, for the purposes of the present work, the previous equation is all what we need to study in the next section the instability problem. However, Eqs. (1), (7), and (8) allow for obtaining the time dependence $p_p(t)$ on the interface necessary

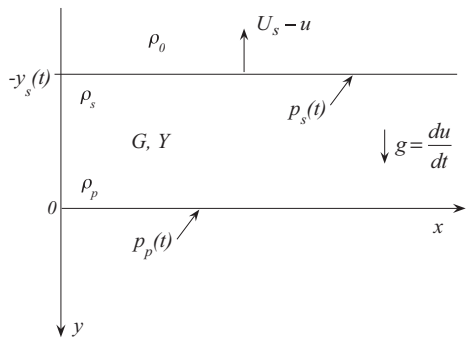

FIG. 1. Diagram of the unperturbed interface ($y = 0$) and of the shock wave ($y = -y_s$) in the interface reference frame.

to drive the constant acceleration flow behind the shock. In fact, from Eq. (8) with $u = g_0 t$, we get

$$y_s = c_0 t + \frac{s-1}{2} g_0 t^2. \tag{11}$$

Taking into account mass conservation, it is $\rho\, dy = \rho(U_s - u)dt = \rho_0 U_s dt$, and $p_p(t)$ results to be

$$p_p(t) = 2\rho_0 c_0 g_0 t \left(1 + \frac{3sg_0}{4c_0} t\right). \tag{12}$$

Different pressure histories on the interface can be obtained by following the same procedure for different assumptions of the time dependence of $u(t)$. But, for the purpose of the present study, the previous picture is very suitable. The only condition is to keep isentropic the flow behind the shock for which, after the shock formation, the characteristic time $t_d = p_p/(dp_p/dt)$ of variation of the driving pressure pulse on the piston must be larger or of the order of the sound waves' transit time t_T between the piston and the shock ($t_d \geqslant t_T$). In this manner, the sequentially launched compression waves from the piston will not overlap, giving place to a new shock behind the first one, and they will just contribute to the intensity enhancement of a single shock wave. For the case of a power law $p_p(t) \sim t^n$, this condition is fulfilled provided that n is not much larger than unity. The particular case $n = 0$ (p_p = constant) was considered in Ref. [29] and leads to uniform pressure and density profiles behind the shock. In the opposite case, when $t_d \ll t_T$ occurs, new shocks are formed and the hypothesis of isentropic flow behind the shock breaks.

In the present case, the previous isentropic flow assumption together with the flat velocity profile approximation in the momentum conservation equation lead to quasihydrostatic profiles between the shock and the piston. The details of such profiles, depending on the equation of state of the solid medium, are not necessary for the present purposes and will be analyzed elsewhere.

B. Instability model

1. Initial phase and RMI

We consider now that the solid free surface has a small sinusoidal corrugation of amplitude ξ_i and wavelength λ which are taken in such a manner that they satisfy the condition $k\xi_i \ll 1$. At the time $t = 0$ a time-dependent pressure $p_p(t)$ is applied at the interface solid-vacuum ($y = 0$) that drives a corrugated shock moving with a velocity $U_s(t)$ into the solid material. If the shock is formed at a distance from the interface larger than k^{-1}, this region will be isentropically accelerated and RTI will affect the interface immediately from $t = 0$, with no influence of RMI.

Instead, when the shock is formed within a distance much shorter than k^{-1}, as in Ref. [29] were a box pressure pulse was applied on the piston surface, then we consider that RMI develops and this corrugated shock produces pressure modulations in the shocked region that impart an acceleration to the ripple modulation of the interface during the time interval $0 \leqslant t \leqslant t_0$ in which the shock is within a distance $y_s \leqslant k^{-1}$ [49].

We will not describe the details of the interaction between the shock and the interface but, instead, we assume that this interaction ends at $t = t_0$ leaving a rotational velocity field behind the shock. As in Refs. [29,30,32,33] we will approximately represent such a velocity field for $t > t_0$ ($y_s > k^{-1}$) in the following form:

$$v_x = \dot{\zeta}(t) e^{q_x y} \cos kx, \quad \dot{\eta} = v_y = \dot{\xi}(t) e^{qy} \sin kx, \tag{13}$$

where η is the vertical component of the medium perturbation, ξ and $\dot{\xi}$ are, respectively, the instantaneous normal amplitude and velocity of the interface, and $\zeta(t)$ and $\dot{\zeta}(t)$ are, respectively, the instantaneous tangential amplitude and velocity of the interface.

In addition, q^{-1} and q_x^{-1} are the characteristic lengths with which the surface modes decay from the interface. As in Ref. [29] we impose them into the model equations in the same manner as has been also done in the past in similar models for RTI and RMI [26–37]. We take $q^{-1} = \alpha k^{-1}$ and $q_x^{-1} = \alpha_x k^{-1}$, where α is a numerical factor that expresses our ignorance about the exact velocity field and that, according to the numerical simulations results of Refs. [28–30], can be taken as $\alpha \approx 1.5$. Besides, the incompressibility of the perturbations requires that $q\dot{\xi} = k\dot{\zeta}$ at $y = 0$, and the parameter $\alpha_x = k/q_x$ will be determined by the self-consistency of the equation of motion for the perturbations [29,30].

When the shock is formed at distance larger than k^{-1} ($t > t_0$) from the interface, the flow in this region is taken as isentropic and the velocity field in Eqs. (13) reduces to the irrotational case ($\alpha = \alpha_x = 1$), and we consider that RMI is not present, so that RTI develops from the very beginning.

Besides, due to the low compressibility of the shocked material we can neglect the change in the corrugation amplitude for $t \leqslant t_0$ and consider that the main effects of this RMI phase are to create the velocity field given by Eq. (13) and to impart a normal velocity $\dot{\xi}_0 = \dot{\xi}(t_0)$ to the interface corrugation amplitude. Therefore, the effects of the mechanical properties of the material can be neglected in this phase and we can assume that $\dot{\xi}_0$ is given by the classical expression for the asymptotic velocity [50,52–54],

$$\dot{\xi}_0 \approx k\xi_0 u(t_0), \tag{14}$$

where, according to the previous discussion, we have taken $\xi_0 = \xi(t_0) \approx \xi_i$, and t_0 is given by the condition that $y_s(t_0) = k^{-1}$. For the case of a constant acceleration g_0 of the interface, we have

$$\dot{\xi}_0 \approx k\xi_0 g_0 t_0, \tag{15}$$

$$t_0 = \frac{c_0}{(s-1)g_0}\left[\sqrt{1 + \frac{2(s-1)g_0}{kc_0^2}} - 1\right]. \tag{16}$$

2. RTI phase

The force driving the RMI, when it is present, lasts only for the relatively short period of time t_0 during which the initial conditions for RTI, such as those given by Eqs. (13) to (16), are settled. The linear evolution of the perturbation amplitude in this latter phase can be described by the following equation of motion for the perturbation amplitude [26–33,35–37,55–60]:

$$\frac{\rho}{q}\ddot{\eta} = \rho g \eta - S_{yy}, \tag{17}$$

where $g = du/dt$ and it will be taken as a constant $g = g_0$. S_{yy} is the normal component of the perturbation of the deviatoric part S_{ij} of the stress tensor $\sigma_{ij} = -p\delta_{ij} + S_{ij}$ (p is the thermodynamic pressure and δ_{ij} is Kronecker delta). We are using the usual tensor notation where i and j denote the coordinate directions x, y, z). In addition, ρ is the solid density in the region close to the interface, and' because of the low compressibility it will be taken as $\rho \approx \rho_0$.

Equation (17) represents the momentum conservation equation for the motion due to the perturbation of the interface, with ρ/q being the mass per unitary surface of the medium that is involved in the motion, and $\ddot{\eta}$ being its acceleration, so that the term on the left-hand side is change of momentum caused by the forces acting on the medium. These forces are given by the terms on the right-hand side of Eq. (17), where the first term ($\rho g \eta$) is the buoyancy force arising when the interface departs from the equilibrium position and a hydrostatic pressure difference is created on the interface. This is the force that drives the instability and defines the RTI. The second term on the right-hand side of Eq. (17), S_{yy}, represents, in general, any other force of either external (like magnetic fields, coriolis effects, etc.) or internal origin (mechanical forces including viscous effects, surface tension, elasticity, etc.). In the framework of RTI, these forces are, by definition, stabilizing forces because the instability is defined by the driving force that causes it.

In the present case, S_{yy} represents the mechanical forces due to the EP material properties of the solid, and it was obtained in Ref. [29] by assuming an EP solid with constitutive properties described by the Prandtl-Reuss model with the von Mises yield criterion [29,30,32,33]:

$$S_{yy} = \begin{cases} 2kGM_{yy}(\eta - \eta_0) & \text{if } \eta \leqslant \eta_p, \\ \sqrt{\frac{2}{3}}\frac{M_{yy}}{|M|}Y & \text{if } \eta \geqslant \eta_p, \end{cases} \tag{18}$$

$$\eta = \xi(t)e^{qy}\sin kx, \tag{19}$$

where $\xi(t)$ is the instantaneous perturbation amplitude of the interface, and η_0 and η_p correspond to the initial and to the EP transition amplitudes, respectively. In addition, G and Y are, respectively, the solid shear modulus and the yield strength, and we have used the following definitions:

$$M_{ij} = \frac{D_{ij}}{k\dot{\xi}}, \quad D_{ij} = \frac{1}{2}\left(\frac{\partial v_i}{\partial x_j} + \frac{\partial v_j}{\partial x_i}\right), \tag{20}$$

$$|M|^2 = M_{xx}^2 + M_{yy}^2 + 2M_{xy}^2. \tag{21}$$

Therefore, from Eq. (13), we get

$$M_{yy} = \frac{1}{\alpha}e^{qy}\sin kx, \quad |M| = \frac{\sqrt{2}}{\alpha}e^{qy}, \tag{22}$$

where we have already considered that the self-consistence of Eq. (17) requires that $|M|$ must be independent of the coordinate x and, therefore, it must be [29]

$$\frac{2}{\alpha^2} = \frac{1}{2}\left(1 + \frac{1}{\alpha\alpha_x}\right)^2. \tag{23}$$

Then, the normal component S_{yy} of the deviatoric part of the stress tensor reads

$$S_{yy} = \begin{cases} \frac{2}{\alpha}kGe^{qy}(\xi - \xi_0)\sin kx & \text{if } \xi \leqslant \xi_p, \\ \frac{1}{\sqrt{3}}Y\sin kx & \text{if } \xi \geqslant \xi_p. \end{cases} \tag{24}$$

Introducing the previous expression into Eq. (17), the equation of motion for the perturbation turns out to be

$$\ddot{\xi} = \frac{k}{\alpha}g\xi - \begin{cases} \frac{2k^2G}{\alpha^2\rho}(\xi - \xi_0) & \text{if } \xi \leqslant \xi_p, \\ \frac{kY}{\sqrt{3}\alpha\rho}e^{q|y_p|} & \text{if } \xi \geqslant \xi_p, \end{cases} \tag{25}$$

where, as in Refs. [33,35–37], we have considered that the onset of plastic flow cannot be felt on the instability until it has affected the entire region with thickness $|y_p| \sim k^{-1}$. In order to agree with the results of the numerical simulations of Refs. [29,33] for the cases of a constant driving pressure and of an irrotational velocity field, respectively, we will take $e^{q|y_p|} \approx 3\alpha$, with $\alpha \approx 1.5$ when the shock is formed within distance shorter than k^{-1} from the interface, and $\alpha \approx 1$ otherwise. Thus, the perturbation equation of motion reads

$$\ddot{\xi} = \frac{k}{\alpha}g\xi - \begin{cases} \frac{2k^2G}{\alpha^2\rho}(\xi - \xi_0) & \text{if } \xi \leqslant \xi_p, \\ \frac{\sqrt{3}kY}{\rho} & \text{if } \xi \geqslant \xi_p. \end{cases} \tag{26}$$

This equation must be solved for $t \geqslant t_0$ with the following initial conditions:

$$\xi(t_0) \approx \xi_0, \quad \dot{\xi}(t_0) \approx \dot{\xi}_0. \tag{27}$$

At this point it is convenient to introduce the following dimensionless magnitudes:

$$z = \frac{\xi - \xi_0}{\xi_0}, \quad \tau = (t - t_0)\sqrt{\frac{kg_0}{\alpha}}, \quad F = \frac{g(t)}{g_0}. \tag{28}$$

Thus, Eq. (26) yields

$$\ddot{z} = F(z+1) - \begin{cases} z/\hat{\lambda} & \text{if } z \leqslant z_p, \\ 1/\hat{\xi} & \text{if } z \geqslant z_p, \end{cases} \tag{29}$$

where

$$\hat{\lambda} = \frac{\alpha\rho g_0\lambda}{4\pi G}, \quad \hat{\xi} = \frac{\rho g_0\xi_0}{\alpha\sqrt{3Y}}, \quad z_p = \frac{\hat{\lambda}}{\hat{\xi}}, \tag{30}$$

and the initial conditions read

$$z(0) \approx 0, \quad \dot{z}(0) \approx \dot{z}_0. \tag{31}$$

For the case of a constant acceleration $g = g_0$ ($F = 1$), we get from Eqs. (15) and (16)

$$\dot{z}_0 = \sqrt{\frac{\alpha}{s-1}}\left(\sqrt{\frac{\mu_0}{\hat{\lambda}} + 2} - \sqrt{\frac{\mu_0}{\hat{\lambda}}}\right), \quad \mu_0 = \frac{\alpha\rho_0 c_0^2}{2(s-1)G}. \tag{32}$$

In Eq. (30) we have introduced the factor $F = g/g_0$ to take into account the situations in which the driving pressure ramp $p_p(t)$ [Eqs. (10) to (12)] switches to a constant pressure ($F = 0$) or decreases producing a negative constant acceleration ($F < 0$) for times $t \geqslant t_R$.

C. Model results for $F = 1$ for $t \leqslant t_R$

For this case, Eq. (29) becomes identical to the one used in Ref. [33] for describing RTI in EP solid plates accelerated as a whole at times longer enough that some few sound waves transit times between the shock and the interface, except for the different definitions of $\hat{\lambda}$ and $\hat{\xi}$. In fact, in the present case, these definitions contain the constant parameter α accounting for the rotationality of the perturbed velocity field generated in the previous RMI phase. We proceed to solve this equation as in Ref. [36], and for this end we introduce the following definitions:

$$x_1 = 1 - \Lambda z, \quad x_2 = z - X, \tag{33}$$

where

$$\Lambda = \hat{\lambda}^{-1} - 1, \quad X = \hat{\xi}^{-1} - 1. \tag{34}$$

Therefore, Eq. (29) is re-written as follows:

$$\ddot{x}_1 = -\Lambda x_1 \quad \text{if } z \leqslant z_p, \tag{35}$$

$$\ddot{x}_2 = x_2 \quad \text{if } z \geqslant z_p; \tag{36}$$

and the initial conditions read:

$$x_1(0) \approx 1, \quad \dot{x}_1(0) \approx -\Lambda \dot{z}_0, \tag{37}$$

$$x_1(\tau_p) = x_2(\tau_p) \equiv x_p, \tag{38}$$

$$\dot{x}_1(\tau_p) \equiv \dot{x}_{1p}, \tag{39}$$

where τ_p is the time when the EP transition takes place.

Equations (35) to (39) will be analytically solved to obtain the complete evolution of the perturbation amplitude in the linear regime. However, we will first find the stability region in the space $(\hat{\lambda},\hat{\xi})$ with $\dot{z}_0$ as a parameter in order to analyze the effects introduced by the early phase dominated by the RMI.

1. Stability boundary

As discussed in Refs. [33,35–37], the boundary for marginal stability is given by the condition that when at a certain time τ_m^{th} it is $\dot{z}(\tau_m^{th}) = 0$, it must also be $\ddot{z}(\tau_m^{th}) = 0$. The index th denotes that we are considering the solutions of Eq. (29) that lie on the instability threshold, and τ_m^{th} is the time when such solutions reach the maximum perturbation amplitude. Equation (29) shows that the conditions for marginal stability are never satisfied for $\hat{\lambda} > 1$ ($z \geqslant 0$) and that stability is only possible for $\hat{\lambda} \leqslant 1$. In order to find the stability boundary we need to integrate Eqs. (35) and (36). For the branch $z \leqslant z_p$ and with the initial conditions given by Eq. (37), we get

$$\dot{x}_1 = -\sqrt{\Lambda\left(1 - x_1^2\right) + \Lambda^2 \dot{z}_0^2} = -\Lambda \dot{z}_p. \tag{40}$$

In a similar manner, upon integration of Eq. (36) with the initial conditions given by Eq. (38), we get

$$\dot{x}_2^2 = \dot{x}_{2p}^2 + x_2^2 - x_p^2. \tag{41}$$

Since on the instability threshold $\dot{x}_2(\tau_m^{th}) = \dot{z}(\tau_m^{th}) = 0$ and $\ddot{x}_2(\tau_m^{th}) = \ddot{z}(\tau_m^{th}) = 0$, then Eq. (36) shows that we must also have $x_2(\tau_m^{th}) = 0$. Therefore, Eq. (41) yields

$$\dot{x}_{2p}^{th} = \dot{z}_p^{th} = -x_p^{th}, \tag{42}$$

and, replacing it into Eq. (40) evaluated at $\tau = \tau_p^{th}$, we get

$$x_p^{th} = -\sqrt{\hat{\lambda}\left(1 + \Lambda \dot{z}_0^2\right)}; \tag{43}$$

and, taking into account that $x_p^{th} = 1 - (1 - \hat{\lambda})/\hat{\xi}_{th}$, we obtain the following expression for the stability boundary:

$$\hat{\xi}_{th} = \frac{1 - \hat{\lambda}}{1 + \sqrt{\hat{\lambda} + (1 - \hat{\lambda})\dot{z}_0^2}}, \tag{44}$$

which for $\dot{z}_0 = 0$ reduces to the expression obtained in Ref. [33].

In a similar manner we can find the boundary $\hat{\xi}_{ep}$ for the EP transition by considering that it occurs when the maximum amplitude z_m^e of the pure elastic oscillations (for $z \leqslant z_p$) becomes equal to z_p:

$$\hat{\xi}_{ep} = \frac{1 - \hat{\lambda}}{1 + \sqrt{1 + \frac{1-\hat{\lambda}}{\hat{\lambda}} \dot{z}_0^2}}. \tag{45}$$

We have represented $\hat{\xi}_{th}$ and $\hat{\xi}_{ep}$ in Fig. 2 for different values of the parameter μ_0 defined by Eq. (32) that accounts for the initial velocity $\dot{z}_0$. As we can see, the effect of the initial velocity is to reduce both the region of stability and the region below the EP boundary. However, for typical cases it is $\mu_0 > 2$. For instance it is $\mu_0 = 6.2$ for Al and W, and therefore the results do not differ considerably from the case for $\dot{z}_0 = 0$. However, we should remember that the present definitions of the parameters $\hat{\lambda}$ and $\hat{\xi}$ differ from the ones corresponding to the irrotational case of Ref. [33] in the factor $\alpha \approx 1.5$. Thus, in the present case the maximum stable wavelength is reduced by a such a factor α, while the maximum stable initial amplitude (for $\hat{\lambda} = 0$) is increased by the same factor. It seems that the main effect of initial RMI phase on the stability boundary comes from the modification of the perturbed velocity field that is found when the RTI develops.

2. Evolution of the perturbation amplitude

From Fig. 2(A) we can see that, as in the case of pure RTI of Ref. [33], here we also have two kinds of stable solutions occurring both for $\hat{\lambda} < 1$: one for $0 \leqslant \hat{\xi} \leqslant \hat{\xi}_{ep}$ that corresponds to pure elastic solutions, and the other one for $\hat{\xi}_{ep} \leqslant \hat{\xi} \leqslant \hat{\xi}_{th}$ which corresponds to solutions that, after undergoing the transition to the plastic regime, achieve a maximum and then go back to an oscillatory elastic regime.

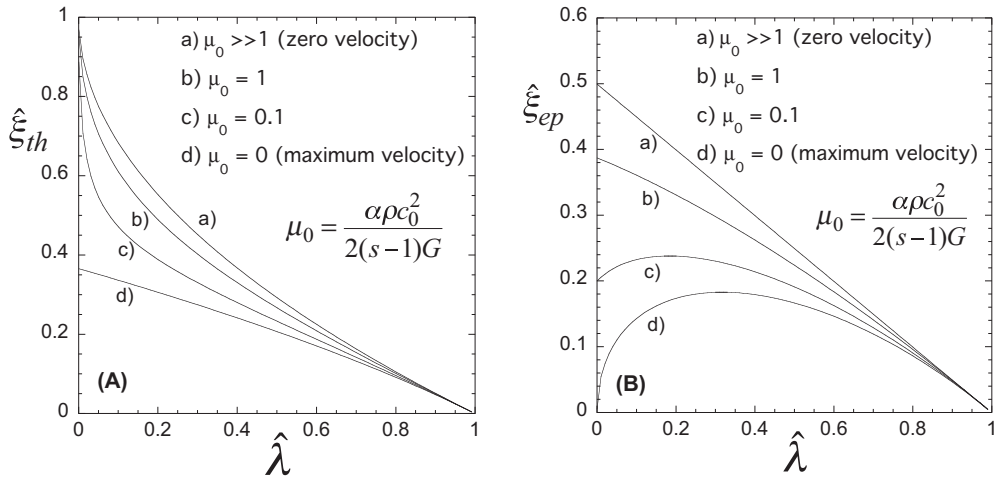

FIG. 2. Dimensionless amplitude $\hat{\xi}$ as a function of the dimensionless perturbation wavelength $\hat{\lambda}$ for (A) the stability boundary and (B) the EP transition boundary $\hat{\xi}_{ep}$, for different values of the parameter μ_0 determining the initial perturbation velocity.

These stable solutions are given by the following expressions:

$$z(\tau)=\begin{cases}\frac{1}{\Lambda}[1-\cos(\sqrt{\Lambda}\,\tau)+\dot{z}_0\sqrt{\Lambda}\sin(\sqrt{\Lambda}\,\tau)], & \tau\leqslant\tau_p,\\ X+\frac{1}{2}[(x_p+\dot{x}_{2p})e^{(\tau-\tau_p)}+(x_p-\dot{x}_{2p})e^{-(\tau-\tau_p)}], & \tau_p\leqslant\tau\leqslant\tau_m,\\ z_m-\frac{X-z_m}{\Lambda}\{1-\cos[\sqrt{\Lambda}(\tau-\tau_m)]\}, & \tau\geqslant\tau_m,\end{cases}\tag{46}$$

where $x_{1p}=1-\Lambda z_p$, and $\dot{x}_{2p}=\dot{z}_p=-\dot{x}_{1p}/\Lambda$ is given by Eq. (40) evaluated at $\tau=\tau_p$:

$$\dot{x}_{2p}=\sqrt{\dot{z}_0^2+\frac{1-(1-\Lambda z_p)^2}{\Lambda}},\tag{47}$$

and τ_p is given by the following implicit equation:

$$\Lambda z_p=1-\cos(\sqrt{\Lambda}\,\tau_p)+\dot{z}_0\sqrt{\Lambda}\sin(\sqrt{\Lambda}\,\tau_p).\tag{48}$$

In addition, we have

$$\tau_m=\tau_p+\frac{1}{2}\ln\frac{x_p-\dot{x}_{2p}}{x_p+\dot{x}_{2p}},\quad z_m=X+\sqrt{\dot{x}_{2p}^2-x_p^2}.\tag{49}$$

In a similar manner we find that there are two kind of unstable solutions occurring: one for $\hat{\lambda}<1$ and $\hat{\xi}\geqslant\hat{\xi}_{th}$, and the other one occurring for $\hat{\lambda}>1$.

For $\hat{\lambda}<1$ it reads

$$z(\tau)=\begin{cases}\frac{1}{\Lambda}[1-\cos(\sqrt{\Lambda}\,\tau)+\dot{z}_0\sqrt{\Lambda}\sin(\sqrt{\Lambda}\,\tau)], & \tau\leqslant\tau_p\\ X+\frac{1}{2}[(x_p+\dot{x}_{2p})e^{(\tau-\tau_p)}+(x_p-\dot{x}_{2p})e^{-(\tau-\tau_p)}], & \tau\geqslant\tau_p\end{cases}.\tag{50}$$

$$z(\tau)=\begin{cases}\frac{1}{\Lambda}[1-\cosh(\sqrt{-\Lambda}\,\tau)-\dot{z}_0\sqrt{-\Lambda}\sinh(\sqrt{-\Lambda}\,\tau)], & \tau\leqslant\tau_p\\ X+\frac{1}{2}[(x_p+\dot{x}_{2p})e^{(\tau-\tau_p)}+(x_p-\dot{x}_{2p})e^{-(\tau-\tau_p)}], & \tau\geqslant\tau_p\end{cases}.\tag{51}$$

Except for the initial velocity $\dot{z}_0$ at $t=t_0$ ($\tau=0$), the solutions presented in this section are the same as the ones obtained in Ref. [33]. We have represented four typical cases in Fig. 3, each one corresponding to a kind of stable or unstable solution. Here, in order to highlight the effect of changing the acceleration g_0, in Fig. 3 we have used the transformed time $\tau'=\tau/\sqrt{\hat{\lambda}}$ which is independent of g_0. Thus, $\hat{\lambda}$ can be taken here as a dimensionless gravity for a given perturbation wavelength λ.

D. Pressure ramp with $p_p(t)$ = const for $t\geqslant t_R$

Here we consider a driving pressure $p_p(t)$ that generates a constant acceleration g_0 during the time interval $0\leqslant t\leqslant t_R$ and then the acceleration becomes $g(t\geqslant t_R)=0$ ($F=0$). This requires that the pressure behind the shock given by Eq. (10) stops growing at $t=t_R$ and becomes a constant $p_0=p_s(t_R)$. Then, we can obtain the required driving pressure on the interface as in Sec. II A, by assuming $\partial u/\partial y\approx 0$ between the shock and the interface so that $p_p(t)$ is given by Eq. (12) for $t\leqslant t_R$ and $p_p(t\geqslant t_R)=p_0$, thus presenting a discontinuity at $t=t_R$ that reflects the discontinuity of the acceleration such as that shown in Fig. 4.

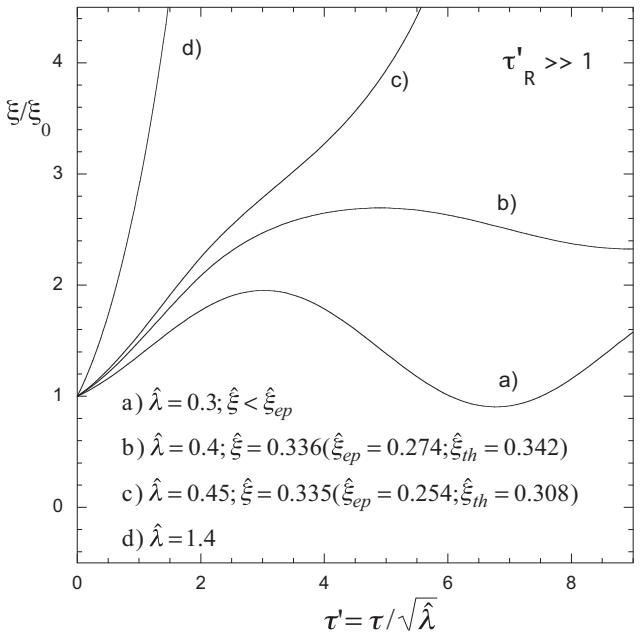

FIG. 3. Perturbation amplitude as a function of time for different values of the dimensionless parameters $\hat{\xi}$ and $\hat{\lambda}$.

We rewrite Eqs. (10) and (12) as follows:

$$\pi_s = T + T^2 \quad \text{for } T \leqslant T_R, \tag{52}$$

$$\pi_p = 2T + \tfrac{3}{2}T^2 \quad \text{for } T \leqslant T_R, \tag{53}$$

where we have used the following definitions:

$$\pi = \frac{sp}{\rho_0 c_0^2}, \quad T = \frac{s g_0 t}{c_0}. \tag{54}$$

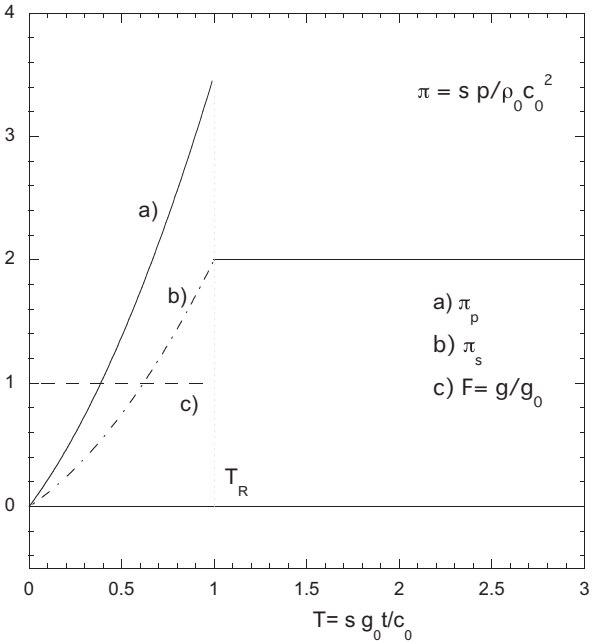

FIG. 4. Time evolutions of the pressures at the interface (π_p), and at the shock (π_s), and of the interface acceleration (F). $F = 0$ for $t > t_R$.

By calling $\pi_0 = \pi_s(T_R)$ we get

$$T_R = \tfrac{1}{2}(\sqrt{1 + 4\pi_0} - 1). \tag{55}$$

Figure 4 shows that $p_p(t) > p_s(t)$ when $dp_p/dt > 0$, as should be expected from the process of shock formation [61–63].

Here we examine the instability evolution for the most interesting case, in which the pressure ramp duration is longer that the time required for the EP transition to take place ($t_R > t_p$). Then, the perturbation evolution for $t \leqslant t_R$ is given by Eqs. (46) to (51) in the previous section. However, we need to contemplate only the unstable solutions, and those stable ones for which $t_R \leqslant t_m$. Therefore, for $t \leqslant t_R$ it is sufficient to consider Eqs. (50) and (51).

On the other hand, for $t \geqslant t_R$ the interface acceleration becomes zero ($F = 0$) and Eq. (29) must be replaced by

$$\ddot{z} = -\begin{cases} z/\hat{\lambda} & \text{if } z \leqslant z_p, \\ 1/\hat{\xi} & \text{if } z \geqslant z_p. \end{cases} \tag{56}$$

This equation must be solved with the condition at $\tau = \tau_R$ [$z(\tau_R) = z_R$, and $\dot{z}(\tau_R) = \dot{z}_R$] left by the previous phase driven by the pressure ramp [Eqs. (52) and (53)]:

$$z_R = X + \tfrac{1}{2}[(x_p + \dot{x}_{2p})e^{(\tau_R - \tau_p)} + (x_p - \dot{x}_{2p})e^{-(\tau_R - \tau_p)}], \tag{57}$$

$$\dot{z}_R = \tfrac{1}{2}[(x_p + \dot{x}_{2p})e^{(\tau_R - \tau_p)} - (x_p - \dot{x}_{2p})e^{-(\tau_R - \tau_p)}]. \tag{58}$$

Since we are assuming that $\tau_R \geqslant \tau_p$, the perturbation is growing in the plastic regime and it will remain in it until the maximum amplitude is achieved at the time τ_{m2}. Therefore, the solution of Eq. (56) reads

$$z(\tau) = \begin{cases} z_R + \dot{z}_R(\tau - \tau_R) - \frac{1}{2\hat{\xi}}(\tau - \tau_R)^2, & \tau_R \leqslant \tau \leqslant \tau_{m2}, \\ z_{m2} - z_p\left[1 - \cos\left(\frac{\tau - \tau_{m2}}{\sqrt{\hat{\lambda}}}\right)\right], & \tau \geqslant \tau_{m2}, \end{cases} \tag{59}$$

where

$$\tau_{m2} = \tau_R + \hat{\xi}\dot{z}_R, \quad z_{m2} = z_R + \tfrac{1}{2}\hat{\xi}\dot{z}_R^2. \tag{60}$$

In Fig. 5 we have represented the perturbation amplitude as a function of the dimensionless time $\tau' = \tau/\sqrt{\hat{\lambda}}$ for two different cases with the same acceleration time τ'_R and, therefore, with the same duration of the driving pressure ramp, but with different final pressures (different accelerations $\hat{\lambda}$), as shown in the inset of the figure where the pressures p_s behind the shock have been represented. We see that the maximum amplitude, as well as the time required to achieve it, increases with the magnitude of the final pressure p_0. This can be better appreciated in Fig. 6 where we have represented the maximum perturbation amplitude z_{m2} and the time τ_{m2} necessary to achieve it as functions of the dimensionless interface acceleration $\hat{\lambda}$ for different durations of the pressure ramp and different ratios z_p between the perturbation wavelength and initial amplitude. We have used a fixed value of the material parameter $\mu_0 = 6$ which is close to the value corresponding to Al and W. Both z_{m2} and τ_{m2} grow monotonically with the driving gravity g_0 ($\hat{\lambda}$).

In Fig. 7 we show the time evolution of the perturbation amplitude for different pressure ramps, so that accelerations g_0 during the time interval $0 \leqslant t \leqslant t_R$ are also different, but

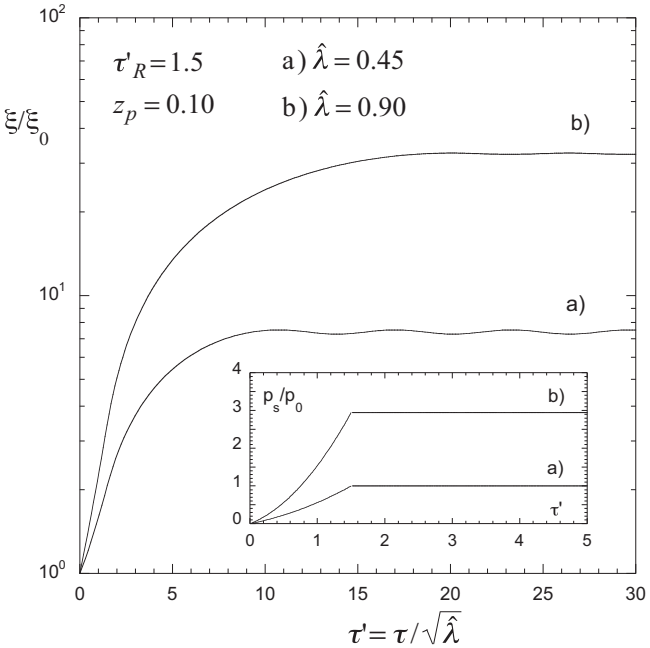

FIG. 5. Time evolution of the perturbation amplitude for two cases with different driving accelerations $\hat{\lambda}$ and with the same duration of the pressure ramp (different final pressures).

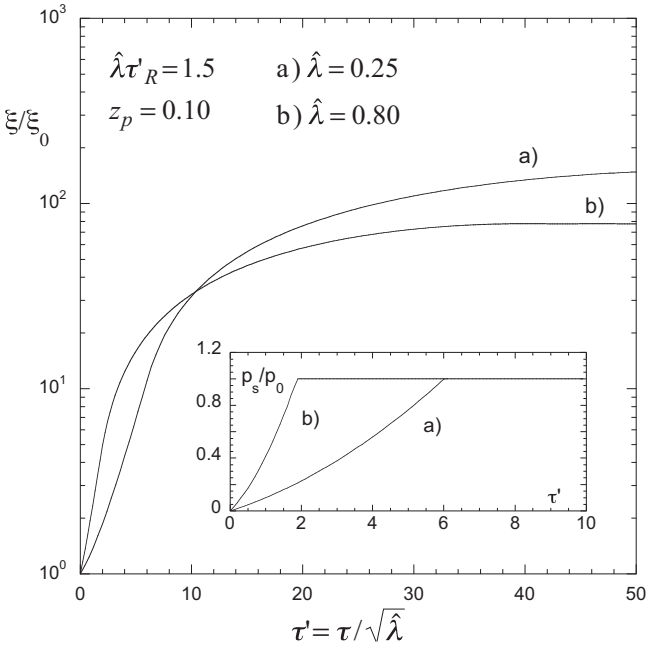

FIG. 7. Time evolution of the perturbation amplitude for two cases with different driving accelerations $\hat{\lambda}$, and different duration of the pressure ramp, but with the same final pressure.

in both cases the final pressure is the same (see the inset). Thus, also the final particle velocity $u_R = g_0 t_R$ is the same. In this case the perturbation amplitude grows more slowly for the case with the lowest acceleration sustained for a longer time, but the maximum amplitude becomes larger. In other words, a shorter ramp leads to a lower maximum amplitude and, in addition, it takes a shorter time to achieve this maximum.

The behaviors shown in Figs. 5 to 7 are qualitatively identical to those observed in the numerical simulations of Ref. [44] for the case of a linear ramp, instead of the parabolic one used here, which is more suitable for an analytical treatment. Nevertheless, the tendency described in Fig. 7 is actually not general, and this can be seen in Fig. 8 representing z_{m2} and τ_{m2} for $u_R = \text{const}$ as a function of the dimensionless driving acceleration $\hat{\lambda}$ acting during the ramp duration ($\tau' \leqslant \tau'_R$). For $\hat{\lambda}\tau' = 1.5$ [Figs. 8(A) and 8(B)] we can see that the behavior observed in Fig. 7 only occurs for some cases with relatively low accelerations ($\hat{\lambda} < 1$). However, by increasing the final particle velocity u_R so that $\hat{\lambda}\tau' = 3$ the

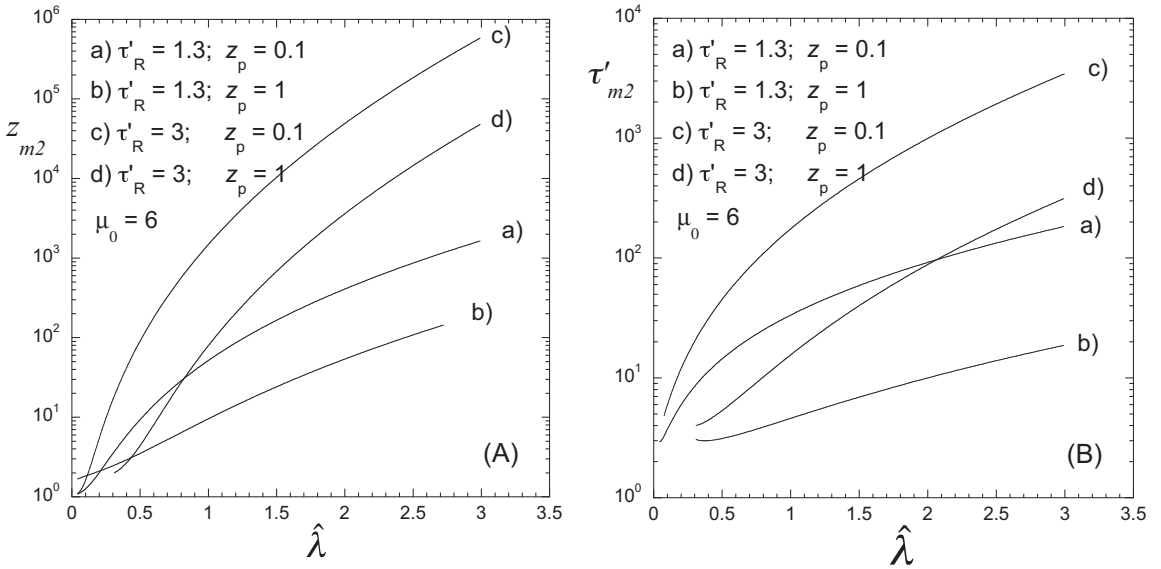

FIG. 6. (A) Maximum perturbation amplitude z_{m2} and (B) time τ_{m2} to achieve the maximum as a function of the interface acceleration $\hat{\lambda}$ for two different durations of the pressure ramp and for different ratios $z_p = \hat{\lambda}/\hat{\xi}$.

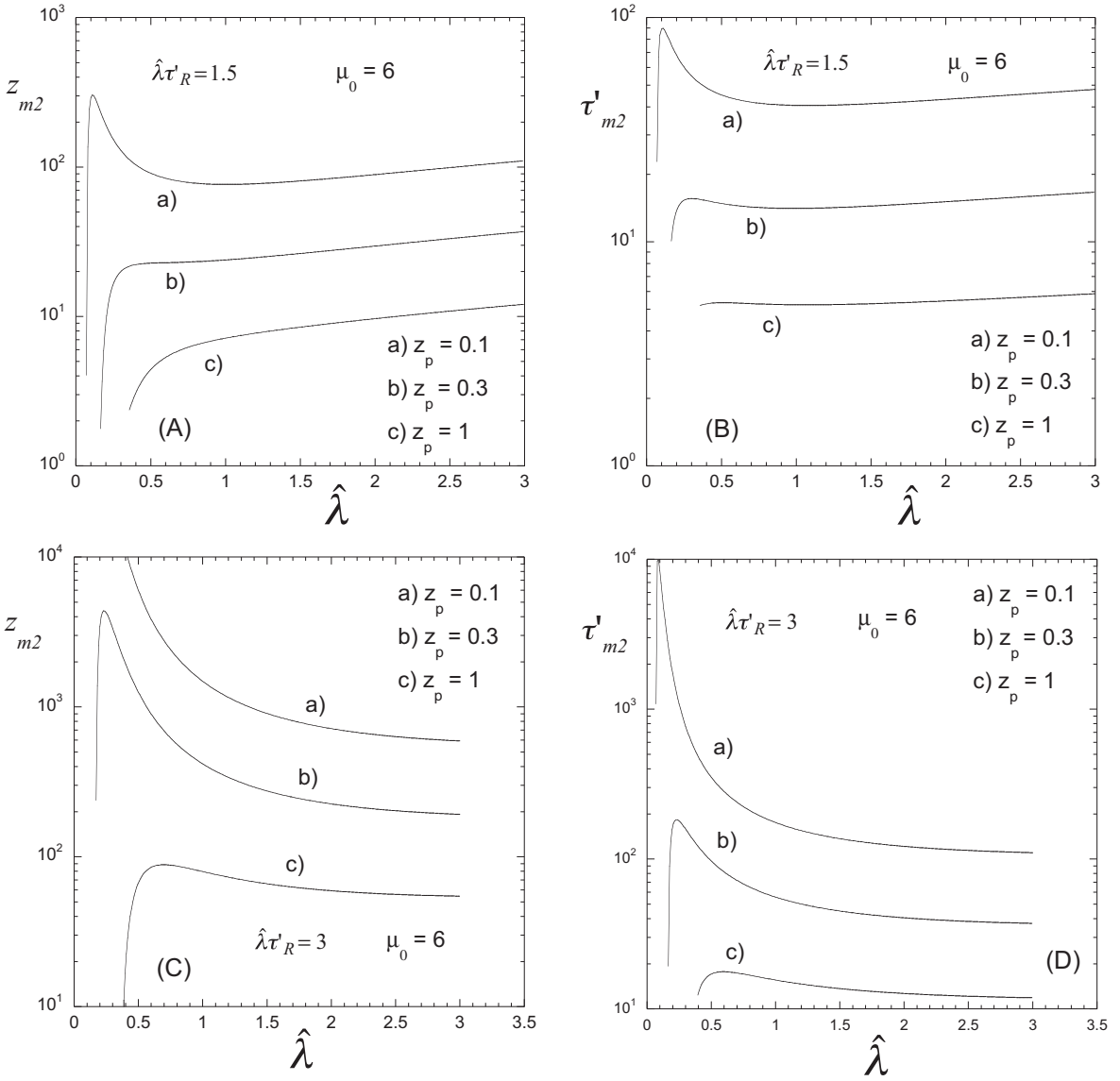

FIG. 8. Maximum perturbation amplitude z_{m2} [(A) and (C)] and time τ_{m2} to achieve the maximum [(B) and (D)] as a function of the interface acceleration $\hat{\lambda}$ for two different velocities at the end of the pressure ramp ($\hat{\lambda}\tau' = 1.5$ and 3), and for different ratios $z_p = \hat{\lambda}/\hat{\xi}$.

behavior shown in Fig. 7 is more pronounced, indicating that the numerical simulation results obtained in Ref. [44] may not be general but are at least quite typical. For a quantitative comparison with the results of Ref. [44] it would have been necessary here to impose a linear time dependence of the driving pressure $p_p(t)$ on the interface, such as what was considered in those numerical simulations. However, as we have already mentioned, it would not have been possible to obtain analytical solutions from the present model, thus obscuring the physical interpretations. On the other hand, detailed comparisons are impossible because, unfortunately, in that paper the specific perturbation wavelengths used in the corresponding calculations are missing, making it impossible to attempt a quantitative comparison.

Anyway, we can at least to compare the orders of magnitude that results from the present model with those of the numerical simulations of Ref. [44]. We show in Table I the values of the physical quantities for an Al sample ($G = 28$ GPa; $Y = 0.3$ GPa, $\rho_0 = 2700$ kg/m^3, $c_0 = 5380$ m/s, and $s = 1.337$), for the two cases represented in Fig. 5. We have chosen a perturbation wavelength $\lambda = 8.89$ mm and an initial perturbation amplitude $\xi_0 = 4$ μm, which correspond to at least one of the cases reported in Ref. [44]. We have assumed

TABLE I. Physical parameters corresponding to the two cases shown in Fig. 5 for an Al solid medium. The perturbation wavelength and initial amplitude are $\tau'_R = 1.5$, with $\lambda = 8.89$ mm, and $\xi_0 = 4$ μm. ($t_0 = 0$, $t_R = 0.466$ μs, $\sqrt{\hat{\lambda}/kg_0} = 0.311$ μs.)

$\hat{\lambda}$	$\xi_{\max}$ (μm)	g_0 (m/s^2)	p_0 (GPa)	p_{pR} (GPa)
(a) 0.45	30	0.66×10^{10}	78	140
(b) 0.90	130	1.32×10^{10}	223	380

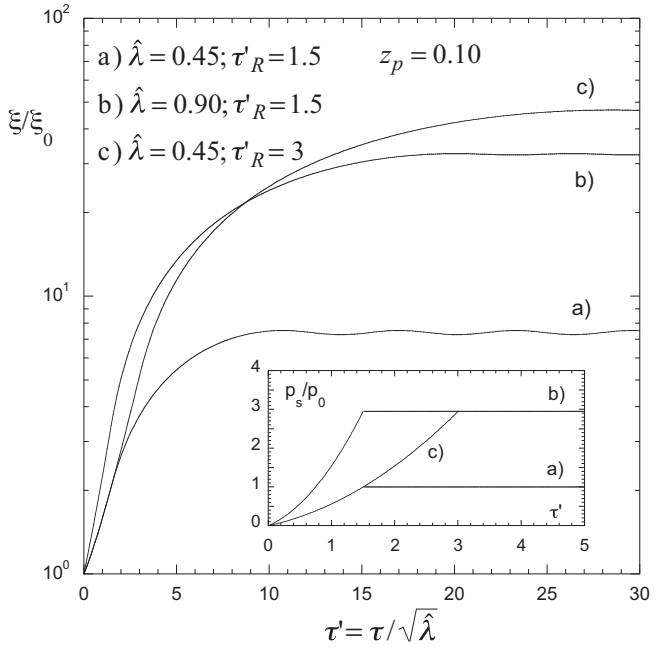

FIG. 9. Time evolution of the perturbation amplitude for two cases with the same driving acceleration $\hat{\lambda}$ and with the different durations of the pressure ramp [curves (a) and (c)], and for a case with the same final pressure as that in curve (b) but with a different pressure ramp.

that the presence of RMI in the initial phase is negligible and we have taken $\alpha = 1$ (irrotational velocity field). The resulting pressure pulse on the interface grows parabolically from $t = 0$ until $t = 0.466$ μs, achieving a maximum value $p_p(t_R) = p_{pR} = 140$ GPa for the case (a) with $\hat{\lambda} = 0.45$, and $p_{pR} = p_p(t_R) = 380$ GPa for the case (b) with $\hat{\lambda} = 0.90$. For $t \geqslant 0.466$ μs the pressures on the interface and behind the shock both become constant and equal to $p_0 = 78$ GPa and $p_0 = 223$ GPa, respectively. The perturbation grows up to values $\xi_{\max} = 30$ μm (at $t_{\max} = 3.4$ μs) and $\xi_{\max} = 130$ μm (at $t_{\max} = 5.9$ μs), respectively.

These values are of the same order of magnitude as the ones presented in Fig. 29 of Ref.[44]. It should be noticed, however, that in case (b) with $\hat{\lambda} = 0.90$ the maximum pressures on the interface and behind the shock could be above the melting pressure for Al, which has been reported in Ref. [64] to be around 120–160 GPa for a single shock. However, this value considerably increases for a quasi-isentropic compression that keeps the temperature below the melt value given by the Lindemann melt law and depends on the pressure history. Nevertheless, we ignore whether melting effects were included or not in the numerical simulations of Ref. [44].

For completeness we have also represented in Fig. 9 the time evolution of the perturbations for two cases with the same pressure ramp (same initial accelerations) but with different ramp durations t_R [curves (a) and (b) in Fig. 9]. As it could be expected from the previous results, the longest ramp leads to a considerably larger maximum amplitude after having the same initial growth rate. For comparison, curve (c) shows a case with the same final pressure as in curve (b), such as that considered in Fig. 7.

E. Pressure ramp with $dp_p(t)/dt < 0$ for $t \geqslant t_R$

It is relevant to study here the case in which the driving pressure decreases after the end of the ramp at $t = t_R$ in order to get insight into the physical interpretation of the numerical simulations results of Ref. [44]. For this, as in the previous section, we consider an idealized acceleration gravity $g(t)$ consisting in a piecewise function with $g(t \leqslant t_R) = g_0$, $g(t_R \leqslant t \leqslant t_F) = -F_0 g_0$. Then, the pressures $p_s(t)$ behind the shock and $p_p(t)$ at the interface for $t \leqslant t_R$ are still given, respectively, by Eqs. (52) and (53). Instead, for $t_R \leqslant t \leqslant t_F$ we find the resulting pressure functions as in Sec. II A, by replacing g_0 in Eq. (9) by $-F_0 g_0$:

$$\pi_s = T_R + F_0(T - T_R) + [T_R + F_0(T - T_R)]^2, \quad (61)$$

$$\pi_p = \pi_s - F_0\left(T_R + \tfrac{1}{2}T_R^2\right) - F_0(1 + T_R)(T - T_R) + \tfrac{1}{2}F_0^2(T - T_R)^2. \quad (62)$$

For $t = t_F$ we get $p_p(t_F) = 0$, and this happens for a finite value $p_{sF} = p_s(t_F)$ of the pressure behind the shock. Once the driven pressure becomes specified [$p_p(t \geqslant t_F) = 0$], it is not possible any longer to prescribe the acceleration and to impose a constant value because it becomes determined by the process of shock attenuation studied in Refs. [61–63]. For the present purpose of performing the instability analysis, it is sufficient to consider the instability evolution for $t \leqslant t_F$, as was done in the numerical simulations of Ref. [44]. We will discuss elsewhere the problem of the decaying of the shock wave for $t \geqslant t_F$ by using the model of Sec. II A.

A typical case has been represented in Fig. 10 for $F_0 = 1/5$, in which we have truncated the calculation at $t = t_F$. As before, the discontinuity of p_p at $t = t_R$ reflects the corresponding discontinuity of the assumed piecewise acceleration function.

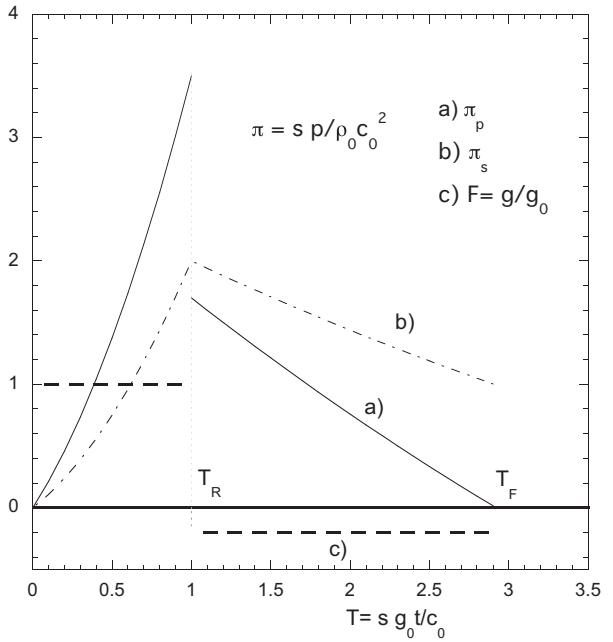

FIG. 10. Time evolutions of the pressures at the interface (π_p) and at the shock (π_s), and of the interface acceleration (F). $F < 0$ for $t_R < t < t_F$ ($F_0 = 0.2$).

Therefore, at the interval $t_R \leqslant t \leqslant t_F$, the perturbation amplitude evolution is obtained by solving Eq. (29) with $F = -F_0$:

$$z(\tau) = \begin{cases} \left(z_R + 1 + \frac{1}{\hat{\xi} F_0}\right) \cos[\sqrt{F_0}\,(\tau - \tau_R)] + \frac{\dot{z}_R}{\sqrt{F_0}} \sin[\sqrt{F_0}\,(\tau - \tau_R)] - 1 - \frac{1}{\hat{\xi} F_0}, & \tau_R \leqslant \tau \leqslant \tau_{m2}, \\ z_{m2} - \frac{z_p + \hat{\lambda} F_0 (z_{m2}+1)}{1+\hat{\lambda} F_0} \left\{1 - \cos\left[\sqrt{F_0 + \frac{1}{\hat{\lambda}}}(\tau - \tau_{m2})\right]\right\}, & \tau_{m2} \leqslant \tau \leqslant \tau_F, \end{cases} \tag{63}$$

where

$$\tau_{m2} = \tau_R + \frac{1}{\sqrt{F_0}} \tan^{-1}\left[\frac{\sqrt{F_0}\dot{z}_R}{F_0(z_R+1) + \hat{\xi}^{-1}}\right]. \tag{64}$$

$$z_{m2} = \frac{1}{F_0}\left\{\sqrt{\left[F_0(z_R+1) + \frac{1}{\hat{\xi}}\right]^2 + F_0 \dot{z}_R^2} - \frac{1}{\hat{\xi}}\right\}. \tag{65}$$

In Fig. 11 we have represented the evolution of the perturbation amplitude for the cases in which the driving pressure remains constant and when it decreases for $t \geqslant t_R$. When the pressure decreases we can observe a strong reduction of the amplitude during the time $t_F - t_R$ in which the pressure decreases to zero. This is again in qualitative agreement with the behavior obtained from numerical simulations in Ref. [44]. This amplitude reduction is a consequence of the large amplitude of the elastic oscillations taking place for $\tau_{m2} \leqslant \tau \leqslant \tau_F$ [see the second branch of Eq. (63)] and of the relatively short decreasing time $t_F - t_R$ of the pressure, in comparison with the period of such oscillations. In fact, the perturbation has no time to grow again before the driving pressure goes to zero at $t = t_F$. Nevertheless, the behavior observed in Fig. 11 depends on the particular choice of the parameters $\hat{\lambda}$, $\hat{\xi}$, and F_0.

In fact, the situation is different in the case shown in Fig. 12 for the same pressure pulses but for a much smaller $\hat{\lambda}$ that results in a higher frequency of the elastic oscillations. As a result, the amplitudes of the elastic oscillations during the interval $\tau_{m2} \leqslant \tau \leqslant \tau_F$ are very similar for both pressure pulses, with constant and with decreasing pressure for $t \geqslant t_R$. The ratio of oscillation amplitudes $A_{\text{const}}/A_{\text{neg}}$ in the elastic regime ($t \geqslant t_{m2}$) for the cases of constant and decreasing pressures for $t \geqslant t_R$, can be obtained from the second branches of Eqs. (59) and (63),

$$\frac{A_{\text{const}}}{A_{\text{neg}}} = \frac{1 + \hat{\lambda} F_0 (z_{m2}+1)/z_p}{1 + \hat{\lambda} F_0}, \tag{66}$$

and the ratio of oscillation frequencies $\omega_{\text{const}}/\omega_{\text{neg}}$ are

$$\frac{\omega_{\text{const}}}{\omega_{\text{neg}}} = \sqrt{1 + \hat{\lambda} F_0}. \tag{67}$$

Then, when $\hat{\lambda} F_0 \ll 1$ both cases becomes very similar, as shown in Fig. 12.

III. CONCLUDING REMARKS

We have presented a model for the RTI occurring at the early stage of acceleration of a solid plate, during the time in which a shock wave driven by a time-varying driving pressure is still

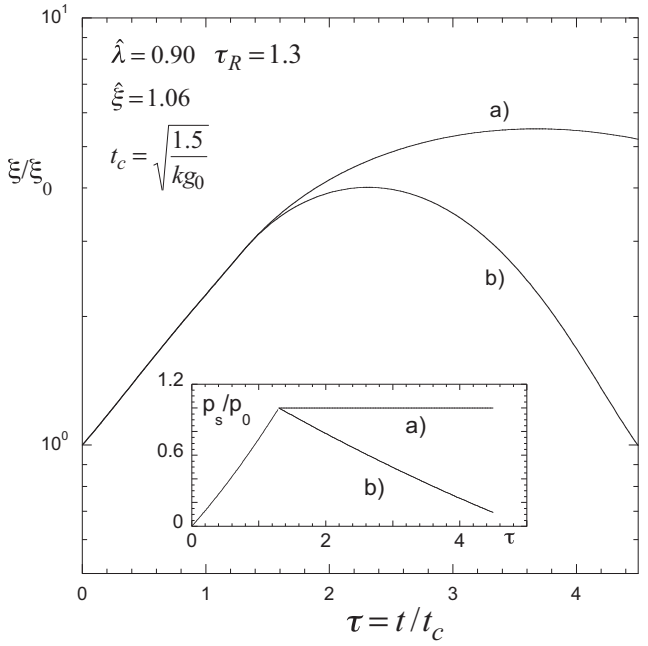

FIG. 11. Time evolution of the perturbation amplitude for two cases with the same driving acceleration $\hat{\lambda}$ for $\tau \leqslant \tau_R$ and with the different evolutions for $\tau \leqslant \tau_R$: constant pressure [curve (a)], and decreasing pressure [curve (b)]. $F_0 = 0.35$, $\hat{\lambda} = 0.90$, and $\hat{\xi} = 1.06$.

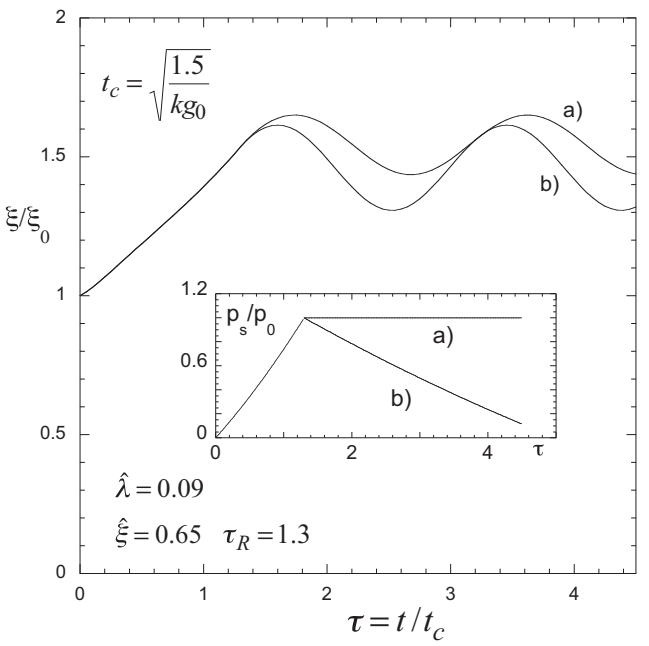

FIG. 12. Time evolution of the perturbation amplitude for two cases with the same driving acceleration $\hat{\lambda}$ for $\tau \leqslant \tau_R$ and with the different evolutions for $\tau \leqslant \tau_R$: constant pressure [curve (a)], and decreasing pressure [curve (b)]. $F_0 = 0.35$, $\hat{\lambda} = 0.09$, and $\hat{\xi} = 0.65$.

running into the plate. This stage may eventually starts after a short initial phase dominated by the RMI that is considered to finalize when the shock has moved away a distance equal to k^{-1} from the interface, provided that the shock has had time to be formed within such a distance.

In order to keep the model analytically tractable we have assumed a piecewise function for the interface acceleration consisting of constant steps, and we have determined the pressures behind the shock and on the interface necessaries to generate such accelerations by means of a relatively simple physical model. In particular, we have considered three different cases resembling the situations studied in Ref. [44] by means of numerical simulation calculations in order to provide a physical interpretation of such results which were originally interpreted in terms of a new acceleration instability distinct of the classical RTI. Namely, we have studied the cases of a positive acceleration, a positive acceleration followed by no acceleration, and a positive acceleration followed by a negative one.

We have shown that indeed there does exist a quantity like the acceleration of gravity in the interface reference frame associated with the time variation of the pressure behind the shock. In fact, the practically uniform particle velocity behind the shock, arising from the not-very-high compressibility of the shocked material, ensures the existence of practically hydrostatic conditions for the medium affected by the interface instability. Therefore, we are in conditions completely analogous to those giving place to the classical RTI. Perhaps the main difference with the classical case is introduced by the rotational velocity field when the initial RMI stage is present. As a consequence, these initial conditions lead to a reduction of the stability region in the space (λ,ξ_0), but no fundamental phenomena are introduced that could justify defining this instability as something different from RTI, especially because no new driving force needs to be assumed.

We have considered an elastic-plastic solid that is described by the Prandtl-Reuss model with von Mises yield criterion, and it qualitatively reproduces the main features of the instability evolution observed in the numerical simulation for the three cases mentioned above. In particular, the effect of the sign of the pressure gradient is directly related to the sign of the time derivative of the pressure by means of the hydrostatic equation, and this derivative determines the acceleration sign in a natural manner through the momentum conservation across the shock [Eqs. (6) and (9)]. Therefore, an amplitude reduction must be expected if a deceleration phase follows the stage of acceleration (Fig. 11). We find that such an effect will occur provided that the resulting period of the elastic oscillations is not too short compared with the duration of this deceleration phase.

The present model can be easily generalized to include an arbitrary time dependence of the driving pressure, provided that the flow behind the shock wave remains isentropic, and/or for considering the compressibility of the shocked material.

ACKNOWLEDGMENTS

This work has been partially supported by the Ministerio de Economía y Competitividad (Grant No. ENE2013-45661-C2-1-P) and by the JCCLM of Spain (Grant No. PEII 11-0056-1890), by the BMBF of Germany, and by the Chinese Academy of Sciences.

[1] S. M. Bakhrakh, O. B. Drennov, N. P. Kovalev, A. I. Lebedev, E. E. Meshkov, A. L. Mikhailov, N. V. Neumerzhitsky, P. N. Nizovtsev, V. A. Rayevsky, G. P. Simonov, V. P. Solovyev, and I. G. Zhidov, Lawrence Livermore National Laboratory Report No. UCRL-CR-126710, 1997 (unpublished).

[2] G. Dimonte, R. Gore, and M. Schneider, Phys. Rev. Lett. **80**, 1212 (1998).

[3] D. H. Kalantar, B. A. Remington, J. D. Colvin, K. O. Mikaelian, S. V. Weber, L. G. Wiley, J. S. Wark, A. Loveridge, A. M. Allen, A. A. Hauer, and M. A. Meyers, Phys. Plasmas **7**, 1999 (2000).

[4] J. D. Colvin, M. Legrand, B. A. Remington, G. Shurtz, and S. V. Weber, J. Appl. Phys. **93**, 5287 (2003).

[5] B. A. Remington, P. Allen, E. M. Bringa, J. Hawreliak, D. Ho, K. T. Lorenz, H. Lorenzana, J. M. McNaney, M. A. Meyers, S. W. Pollaine, K. Rosolankova, B. Sadik, M. S. Schneider, D. Swift, J. Wark, and B. Yaakobi, Mater. Sci. Technol. **22**, 474 (2006).

[6] K. O. Mikaelian, Phys. Plasmas **17**, 092701 (2010).

[7] H-S. Park, K. T. Lorenz, R. M. Cavallo, S. M. Pollaine, S. T. Prisbrey, R. E. Rudd, R. C. Becker, J. V. Bernier, and B. A. Remington, Phys. Rev. Lett. **104**, 135504 (2010).

[8] N. A. Tahir, D. H. H. Hoffmann, A. Kozyreva, A. Tauschwitz, A. Shutov, J. A. Maruhn, P. Spiller, U. Neuner, J. Jacoby, M. Roth, R. Bock, H. Juranek, and R. Redmer, Phys. Rev. E **63**, 016402 (2000).

[9] N. A. Tahir, H. Juranek, A. Shutov, R. Redmer, A. R. Piriz, M. Temporal, D. Varentsov, S. Udrea, D. H. H. Hoffmann, C. Deutsch, I. Lomonosov, and V. E. Fortov, Phys. Rev. B **67**, 184101 (2003).

[10] N. A. Tahir, A. Shutov, D. Varentsov, P. Spiller, S. Udrea, D. H. H. Hoffmann, I. Lomonosov, J. Wieser, M. Kirk, R. Piriz, V. E. Fortov, and R. Bock, Phys. Rev. ST Accel. Beams **6**, 020101 (2003).

[11] M. Temporal, A. R. Piriz, N. Grandjouan, N. A. Tahir, and D. H. H. Hoffmann, Laser Part. Beams **21**, 609 (2003).

[12] N. A. Tahir, P. Spiller, S. Udrea, C. Deutsch, V. E. Fortov, V. Gryaznov, D. H. H. Hoffmann, I. V. Lomonosov, P. Ni, A. R. Piriz, A. Shutov, M. Temporal, and D. Varentsov, Nucl. Instrum. Methods Phys. Res. B **245**, 85 (2006).

[13] N. A. Tahir, Th. Stoehlker, A. Shutov, I. V. Lomonosov, V. E. Fortov, M. French, N. Nettelmann, R. Redmer, A. R. Piriz, C. Deutsch, Y. Zhao, P. Zhang, H. Xu, G. Xiao, and W. Zhan, New J. Phys. **12**, 073022 (2010).

[14] J. F. Barnes, P. J. Blewet, R. G. McQueen, K. A. Meyer, and D. Venable, J. Appl. Phys. **45**, 727 (1974).

[15] J. F. Barnes, D. H. Janney, R. K. London, K. A. Meyer, and D. H. Sharp, J. Appl. Phys. **51**, 4678 (1980).

[16] A. R. Piriz, R. F. Portugues, N. A. Tahir, and D. H. H. Hoffmann, Phys. Rev. E **66**, 056403 (2002).

[17] A. R. Piriz, N. A. Tahir, D. H. H. Hoffmann, and M. Temporal, Phys. Rev. E **67**, 017501 (2003).

[18] A. R. Piriz, M. Temporal, J. J. López Cela, N. A. Tahir, and D. H. H. Hoffmann, Plasma Phys. Contr. Fusion **45**, 1733 (2003).

[19] R. E. Reinovsky, W. E. Anderson, W. L. Atchison, C. E. Ekdahl, R. J. Faehl, I. R. Lindemuth, D. V. Morgan, M. Murillo, J. L. Stokes, and J. S. Shlachter, IEEE Trans. Plasma Sci. **30**, 1764 (2002).

[20] C. A. Hall, J. R. Asay, M. D. Knudsen, W. A. Stygan, R. B. Spielman, T. D. Pointon, D. B. Reisman, A. Toor, and R. C. Cauble, Rev. Sci. Instrum. B **72**, 3587 (2001).

[21] D. B. Sinars, S. A. Slutz, M. C. Herrmann, R. D. McBride, M. E. Cuneo, K. J. Peterson, R. A. Vesey, C. Nakhleh, B. E. Blue, K. Killebrew, D. Schroen, K. Tomlinson, A. D. Edens, M. R. Lopez, I. C. Smith, J. Shores, V. Bigman, G. R. Bennett, B. W. Atherton, M. Savage, W. A. Stygar, G. T. Leifeste, and J. L. Porter, Phys. Rev. Lett. **105**, 185001 (2010).

[22] D. B. Sinars, S. A. Slutz, M. C. Herrmann, R. D. McBride, M. E. Cuneo, C. A. Jennings, J. P. Chittenden, A. L. Velikovich, K. J. Peterson, R. A. Vesey, C. Nakhleh, E. M. Waisman, B. E. Blue, K. Killebrew, D. Schroen, K. Tomlinson, A. D. Edens, M. R. Lopez, I. C. Smith, J. Shores, V. Bigman, G. R. Bennett, B. W. Atherton, M. Savage, W. A. Stygar, G. T. Leifeste, and J. L. Porter, Phys. Plasmas **18**, 056301 (2011).

[23] R. D. McBride, M. R. Martin, R. W. Lemke, J. B. Greenly, C. A. Jennings, D. C. Rovang, D. B. Sinars, M. E. Cuneo, M. C. Herrmann, S. A. Slutz, C. W. Nakhleh, D. D. Ryutov, J.-P. Davis, D. G. Flicker, B. E. Blue, K. Tomlinson, D. Schroen, R. M. Stamm, G. E. Smith, J. K. Moore, T. J. Rogers, G. K. Robertson, R. J. Kamm, I. C. Smith, M. Savage, W. A. Stygar, G. A. Rochau, M. Jones, M. R. Lopez, J. L. Porter, and M. K. Matzen, Phys. Plasmas **20**, 056309 (2013).

[24] B. J. Plohr and D. H. Sharp, Z. Angew. Math. Phys. **49**, 786 (1998).

[25] G. Terrones, Phys. Rev. E **71**, 036306 (2005).

[26] A. R. Piriz, J. J. López Cela, O. D. Cortázar, N. A. Tahir, and D. H. H. Hoffmann, Phys. Rev. E **72**, 056313 (2005).

[27] A. R. Piriz, O. D. Cortazar, J. J. López Cela, and N. A. Tahir, Am. J. Phys. **74**, 1095 (2006).

[28] A. R. Piriz, J. J. López Cela, N. A. Tahir, and D. H. H. Hoffmann, Phys. Rev. E **74**, 037301 (2006).

[29] A. R. Piriz, J. J. López Cela, N. A. Tahir, and D. H. H. Hoffmann, Phys. Rev. E **78**, 056401 (2008).

[30] A. R. Piriz, J. J. López Cela, and N. A. Tahir, Nucl. Instrum. Methods Phys. Res., Sect. A **606**, 139 (2009).

[31] A. R. Piriz, J. J. López Cela, M. C. Serna Moreno, N. A. Tahir, and D. H. H. Hoffmann, Laser Part. Beams **24**, 275 (2006).

[32] A. R. Piriz, J. J. López Cela, and N. A. Tahir, J. Appl. Phys. **105**, 116101 (2009).

[33] A. R. Piriz, J. J. López Cela, and N. A. Tahir, Phys. Rev. E **80**, 046305 (2009).

[34] A. R. Piriz, J. J. López Cela, and N. A. Tahir, Phys. Rev. Lett. **105**, 179601 (2010).

[35] A. R. Piriz, Y. B. Sun, and N. A. Tahir, Phys. Rev. E **88**, 023026 (2013).

[36] A. R. Piriz, Y. B. Sun, and N. A. Tahir, Phys. Rev. E **89**, 063022 (2014).

[37] Y. B. Sun and A. R. Piriz, Phys. Plasmas **21**, 072708 (2014).

[38] N. A. Tahir, A. Kozyreva, P. Spiller, D. H. H. Hoffmann, and A. Shutov, Phys. Rev. E **63**, 036407 (2001).

[39] G. Dimonte, G. Terrones, F. J. Cherne, T. C. Germann, V. Dupont, K. Kadau, W. T. Buttler, D. M. Oro, C. Morris, and D. L. Preston, Phys. Rev. Lett. **107**, 264502 (2011).

[40] W. T. Buttler, D. M. Oro, D. L. Preston, K. O. Mikaelian, F. J. Cherne, R. S. Hixson, F. G. Mariam, C. Morris1, J. B. Stone, G. Terrones, and D. Tupa, J. Fluid Mech. **703**, 60 (2012).

[41] G. Dimonte, G. Terrones, F. J. Cherne, and P. Ramaprabhu, J. Appl. Phys. **113**, 024905 (2013).

[42] M. B. Prime, D. E. Vaughan, D. L. Preston, W. T. Buttler, S. R. Chen, D. M. Oro, and C. Pack, J. Phys.: Conf. Ser. **500**, 112051 (2014).

[43] J.-M. Clarisse, C. Boudesocque-Dubois, and S. Gauthier, J. Fluid. Mech. **609**, 1 (2008).

[44] J. W. Swegle and A. C. Robinson, J. Appl. Phys. **66**, 2838 (1989).

[45] J. G. Wouchuk and K. Nishihara, Phys. Plasmas **3**, 3761 (1996).

[46] J. G. Wouchuk and K. Nishihara, Phys. Plasmas **4**, 1028 (1997).

[47] A. L. Velikovich, J. P. Dahlburg, A. J. Schmitt, J. H. Gardner, L. Phillips, F. L. Cochran, Y. K. Chong, G. Dimonte, and N. Metzler, Phys. Plasmas **7**, 1662 (2000).

[48] V. N. Goncharov, O. V. Gotchev, E. Vianello, T. R. Boehly, J. P. Knauer, P. W. McKenty, P. B. Radha, S. P. Regan, T. C. Sangster, S. Skupsky, V. A. Smalyuk, R. Betti, R. L. McCrory, D. D. Meyerhofer, and C. Cherfils-Clerouin, Phys. Plasmas **13**, 012702 (2006).

[49] M. Lombardini and D. I. Pullin, Phys. Fluids **21**, 044104 (2009).

[50] F. Cobos Campos and J. G. Wouchuk, Phys. Rev. E **90**, 053007 (2014).

[51] R. G. McQueen, S. P. Marsh, J. W. Taylor, J. N. Fritz, and W. J. Carter, in *High Velocity Impact Phenomena*, edited by R. Kinslow (Academic, New York, 1970).

[52] R. D. Richtmyer, Commun. Pure Appl. Math. **13**, 297 (1960).

[53] E. E. Meshkov, Fluid Dyn. **4**, 101 (1969).

[54] K. O. Mikaelian, Phys. Rev. A **42**, 7211 (1990).

[55] S. A. Piriz, A. R. Piriz, and N. A. Tahir, Phys. Plasmas **16**, 082706 (2009).

[56] A. R. Piriz and N. A. Tahir, New J. Phys. **15**, 015013 (2013).

[57] A. R. Piriz, L. DiLucchio, and G. Rodriguez-Prieto, Phys. Plasmas **18**, 012702 (2011).

[58] A. R. Piriz, L. Di Lucchio, G. Rodriguez Prieto, and N. A. Tahir, Phys. Plasmas **18**, 082705 (2011).

[59] A. R. Piriz, S. A. Piriz, and N. A. Tahir, Phys. Plasmas **18**, 092705 (2011).

[60] G. Rodriguez Prieto, A. R. Piriz, J. J. López Cela, and N. A. Tahir, Phys. Plasmas **20**, 012706 (2013).

[61] F. Cottet and J. P. Romain, Phys. Rev. A **25**, 576 (1982).

[62] R. J. Trainor and Y. T. Lee, Phys. Fluids **25**, 1898 (1982).

[63] A. Loeb and S. Eliezer, Phys. Fluids **28**, 1196 (1985).

[64] K. T. Lorenz, M. J. Edwards, S. G. Glendinning, A. F. Jankowski, J. McNaney, S. M. Pollaine, and B. A. Remington, Phys. Plasmas **12**, 056309 (2005).